The anti MRSA biofilm activity of Thymus vulgaris essential oil in nanovesicles

Ana Paula Perez , Noelia Perez , Carlos Mauricio Suligoy Lozano , Maria Julia Altube , Marcelo Alexandre de Farias , Rodrigo Villares Portugal , Fernanda Buzzola , María Jose Morilla , Eder Lilia Romero

PII: S0944-7113(18)30619-6
DOI: https://doi.org/10.1016/j.phymed.2018.12.025
Reference: PHYMED 52802

To appear in: *Phytomedicine*

Received date: 6 November 2018
Revised date: 15 December 2018
Accepted date: 20 December 2018

Please cite this article as: Ana Paula Perez , Noelia Perez , Carlos Mauricio Suligoy Lozano , Maria Julia Altube , Marcelo Alexandre de Farias , Rodrigo Villares Portugal , Fernanda Buzzola , María Jose Morilla , Eder Lilia Romero , The anti MRSA biofilm activity of Thymus vulgaris essential oil in nanovesicles, *Phytomedicine* (2018), doi: https://doi.org/10.1016/j.phymed.2018.12.025

The anti MRSA biofilm activity of *Thymus vulgaris* essential oil in nanovesicles

Ana Paula Perez[a], Noelia Perez[a], Carlos Mauricio Suligoy Lozano[b], Maria Julia Altube[a], Marcelo Alexandre de Farias[c], Rodrigo Villares Portugal[c], Fernanda Buzzola[b], María Jose Morilla[a] and Eder Lilia Romero[a,*]

[a]Nanomedicine Research and Development Centre, Science and Technology Department, National University of Quilmes, Bernal, Buenos Aires, Argentina

[b]Instituto de Investigaciones en Microbiología y Parasitología Médica (IMPaM-CONICET), Departamento de Microbiología, Parasitología e Inmunología, Facultad de Medicina, Universidad de Buenos Aires, Buenos Aires, Argentina.

[c]Brazilian Nanotechnology National Laboratory, CNPEM, Campinas, São Paulo, Brazil

Corresponding author

Eder Lilia Romero

TEL: ++541143657100

FAX: ++541143657132

elromero@unq.edu.ar

Abstract

Background: Thymus vulgaris essential oil (*T*) could be an alternative to classical antibiotics against bacterial biofilms, which show increased tolerance to antibiotics and host defence systems and contribute to the persistence of chronic bacterial infections.

Hypothesis: A nanovesicular formulation of *T* may chemically protect the structure and relative composition of its multiple components, potentially improving its antibacterial and antibiofilm activity.

Study Design: We prepared and structurally characterized *T* in two types of nanovesicles: nanoliposomes (L80-*T*) made of Soybean phosphatidylcholine (SPC) and Polysorbate 80 (P80) [SPC:P80:*T* 1:0.75:0.3 w:w], and nanoarchaeosomes (A80-*T*) made of SPC, P80 and total polar archaeolipids (TPA) extracted from archaebacteria *Halorubrum tebenquichense* [SPC:TPA:P80:*T* 0.5:0.50.75:0.7 w:w]. We determined the macrophage cytotoxicity and the antibacterial activity against *Staphylococcus aureus* ATCC 25923 and four MRSA clinical strains.

Results: L80-*T* (Z potential -4.1 ± 0.6 mV, ~ 115 nm, ~ 22 mg/ml *T)* and A80-*T* (Z potential -6.6 ± 1.5 mV, ~ 130 nm, ~ 42 mg/ml *T)* were colloidally and chemically stable, maintaining size, PDI, Z potential and *T* concentration for at least 90 days. While MIC_{90} of L80-*T* was > 4 mg/ml *T*, MIC_{90} of A80-*T* was 2 mg/ml *T* for all *S. aureus* strains. The antibiofilm formation activity was maximal for A80-*T*, while L80-*T* did not inhibit biofilm formation compared to untreated control. A80-*T* significantly decreased the biomass of preformed biofilms of *S. aureus* ATCC 25923 strain and of 3 of the 4 clinical MRSA isolates at 4 mg/ml *T*. It was found that the viability of J774A.1 macrophages was decreased significantly upon 24 h incubation with A80-*T*, L80-*T* and *T* emulsion at 0.4 mg/ml *T*. These results show that from 0.4 mg/ml *T*, a value lower than MIC_{90} and the one displaying antibiofilm activity, with independence of its formulation, *T* significantly decreased the macrophages viability.

Conclusions: Overall, because of its lower MIC_{90} against planktonic bacteria, higher antibiofilm formation capacity and stability during storage, A80-*T* resulted better antibacterial agent than *T* emulsion and L80-*T*. These results open new avenues to explode the A80-*T* antimicrobial intracellular activity.

Keywords

Thymus vulgaris essential oil, nanovesicles, antibiofilm activity

Abbreviations

A80, nanoarchaeosomes; Abs, absorbance; ATCC, American Type Culture Collection; CFU, colony forming units; cryo-TEM, cryo-transmission electron microscopy; DLS, dynamic light scattering; DSC, differential scanning calorimetry; EO, essential oil; FBS, Fetal bovine serum; GC/MS, gas chromatography/mass spectrometry; GRAS, generally regarded as safe; INTI, National Institute of Industrial Technology; ISO, International Organization for Standardization; L80, nanoliposomes; MBC, minimum bactericidal concentration; MIC_{90}, minimum inhibitory concentration 90; MRSA, methicillin-resistant *Staphylococcus aureus;* OD, optical density; P80, Tween 80; PALS, phase analysis light scattering; PBS, phosphate buffer saline; PDI, polydispersity index; PL, phospholipids; SPC, Soybean phosphatidylcholine; *T*, *Thymus vulgaris* essential oil; TPA, Total polar archaeolipids; T_{RP}, *Thymus vulgaris* essential oil submitted to reduced pressure; TSB, Tryptic soy broth; Tt, phase transition temperature

Introduction

As defined by the International Organization for Standardization (ISO), the term "essential oil" (EO) is reserved for a "product obtained from vegetable raw material, either by distillation with water or steam, or from the epicarp of citrus fruits by a mechanical process or by dry distillation" (ISO 9235, 1997), that is, by physical means only. Many individual components of EOs are generally regarded as safe (GRAS) by the FDA, a status that permitted the use of EOs as flavouring agents in food and as additives to cosmetics, perfumes, and cleaning products (Swamy et al., 2016).

EOs constituents are lipophilic, highly volatile, secondary plant metabolites, reaching a mass below a molecular weight of 300, and have shown different antimicrobial properties against Gram-positive and negative bacteria and fungi (Swamy et al., 2016). Therefore, the antimicrobial activity of EO is associated to their lipophilic components, which may disrupt the lipid bilayer, increase cell permeability to end up in bacterial lysis. Those EOs with a high percentage of phenolic compounds possess the strongest antibacterial properties (Swamy et al., 2016). The constituents of EOs can act synergistically (phyto-synergic interactions) by different mechanisms which significantly reduce the possibility of occurrence of resistance. Interaction among compounds in the EO can involve the protection of an active substance from degradation by enzymes from the pathogen or the modification of transport across cell bilayer, enabling the circumvention of numerous multi-drug resistance mechanisms

based on expulsion of antibiotic molecules ionic bomb-mediated (Bassolé and Juliani, 2012). EOs thus may play a role in the search for new alternatives to classical antibiotics (Rai et al., 2017).

The use of EO as antimicrobials however, is hampered by their low water solubility, chemical instability, photo lability, thermosensitivity and volatility. Nonetheless, such inconveniences may be reduced by loading EO into nanoparticulate material, a strategy aimed to protect the structure of carried drugs against physico-chemical and enzymatic attacks, and also to increase their shelf life, modify their pharmacokinetics, biodistribution and toxicological profile (Rai et al, 2017). One of the priority objectives of the WHO is finding new agents active against resistant bacteria, including methicillin-resistant *Staphylococcus aureus* (MRSA) (WHO, 2017). Once established, the *S. aureus* biofilms are refractory to antimicrobial and immune host response, constituting the etiological agent of recurrent infections. A nanovesicular formulation of EOs may chemically protect the structure and relative composition of its multiple components, potentially improving its antibacterial and antibiofilm activity, enabling its use beyond the food and cosmetic fields.

In this work, *Thymus vulgaris* L. (Lamiaceae) EO (*T)* will be formulated into lipid nanovesicles prepared from polar archaeolipids extracted from the hyperhalophylic archaebacteria *Halorubrum tebenquichense*. In water media, polar archaeolipids form archaeosomes or nanoarchaeosomes, micrometer or submicrometer mean sized nanovesicles, respectively. Nanoarchaeosomes chemically differ from liposomes made of phospholipids (PL) extracted from bacteria and eukaryotes. Opposite to PL, the diphytanylglycerol diethers display *sn*2,3 stereoisomerism and fully saturated polyprenol chains are linked by ether instead of esters bond to the glycerol backbone. Different types of archaeolipids-containing soft colloidal nanostructures have repeatedly shown increased resistance to multiple insults such as mechanical stress, chemoenzymatic hydrolysis and oxidation, improving the protection to the carried drugs (Caimi et al, 2017 and 2019; Altube et al, 2016 and 2017). We hypothesize that *T* formulated in archaeolipid-containing nanovesicles would display improved structural protection during handling and storage, a fact that may help to increase its antimicrobial activity. A structural characterization of *T* loaded in nanoarchaeosomes will be provided and its activity against planktonic and biofilms forming strains of MSRA will be screened.

Materials and methods

Materials

T was obtained from Euma, Buenos Aires, Argentina (density of *T* was considered 0,915 g/ml). Soybean phosphatidylcholine (SPC, purity >90%) was a gift from Lipoid, Ludwigshafen, Germany. Polysorbate 80 (P80), molybdenum oxide, ascorbic acid, Sephadex G-25, 6-dodecanoyl-N, N-dimethyl-2-naphthylamine (laurdan), vancomycin, 3-(4,5-dimethylthiazol- 2-yl)-2,5-diphenyl tetrazolium bromide (MTT) and crystal violet were purchased from Sigma-Aldrich (St Louis, MO, USA). Roswell Park Memorial Institute (RPMI) 1640 medium was from Gibco (Buenos Aires, Argentina). Fetal bovine serum (FBS), antibiotic/antimycotic solution (penicillin 10,000 IU/ml, streptomycin sulphate 10 mg/mL, amphotericin B 25 µg/ml), glutamine, and trypsin/ethylenediaminetetraacetic acid were from PAA Laboratories GmbH (Pasching, Austria). Tryptic soy broth (TSB) and bacteriological agar were acquired from Britania, Buenos Aires, Argentina. The other reagents were of analytic grade from Anedra (Buenos Aires, Argentina), Research AG (Tigre, Buenos Aires, Argentina).

Characterization of T by gas chromatography/mass spectrometry

The composition of *T*, and of *T* submitted to reduce pressure at 25 °C for 30 min (T_{RP}) was analysed by gas chromatography/mass spectrometry (GC/MS). The GC/MS analysis was carried out in the Chemistry Centre of the National Institute of Industrial Technology (INTI, Buenos Aires, Argentina) on a Shimadzu GC 2010 Plus gas chromatograph coupled to a Shimadzu QP2010 ultra selective mass detector. Injector temperature was 250 °C in split mode (split ratio 1:60). The GC column was HP-PONA (50 m x 0.32 mm x 0.25 µm). Helium was used as carrier gas with a constant flow of 1.66 ml/min. The temperature of the column was kept at 50° C for 3 min and was then raised to 230 °C (8 °C/min). Identification of individual components was made by comparison of their retention times with those of analytical standards and by matching mass spectral data with those held in Wiley/NBS Library and NIST11 mass spectral database.

Archaebacteria growth, extraction, and characterization of total polar archaeolipids

Halorubrum tebenquichense archaea were grown using a 25 l home-made stainless-steel bioreactor in basal medium supplemented with yeast extract and glucose at 37 °C (Gonzalez, et al, 2009). Total polar archaeolipids (TPA) were extracted from biomass using the Bligh and Dyer method modified for extreme halophiles (Gonzalez, et al, 2009). The reproducibility of each TPA-extract composition was routinely screened by phosphate content (Böttcher et al, 1961), and electrospray-ionization mass spectrometry, as described in Higa et al., 2012.

Preparation of T-containing nanovesicles

T containing ordinary liposomes (made of SPC:P80, L80-*T*) and nanoarchaeosomes (made of SPC:TPA:P80, A80-*T*) were prepared by the thin-film hydration method. Briefly, SPC, TPA, P80 and *T* were dissolved in CH_3OH:$CHCl_3$ 1:1 v:v and combined in different proportions (SPC:P80:*T* 1:0.5:0.3, 1:0.5:0.7, 1:0.75:0.3, 1:0.75:0.7 w:w; and SPC:TPA:P80:*T* 0.5:0.50.75:0.7 w:w) to obtain suspensions of 40 or 80 mg/ml of PL. Then solvents were evaporated under reduced pressure at 25 °C for 30 min. The film was then hydrated with 10 mM Tris-HCl buffer pH 7.4 with 0.9% w/v NaCl (Tris-HCl buffer).

Nanovesicles with the highest concentration of *T* were extruded 10 times through a sandwich of 2 polycarbonate membranes of 200 and 100 nm pore size, using a Thermobarrel extruder (Northern Lipids, Vancouver, Canada).

Empty nanovesicles (L80 and A80) were prepared by the same procedure without the addition of *T*. A freshly prepared 55 mg/ml T_{RP} in Tris-HCl buffer with 1% w/v of P80 emulsion was used as control (*T* emulsion).

Characterization of T-nanovesicles

Composition and quantification of T, quantification of PL, size and Z potential

T composition upon loaded in nanovesicles was determined by GC/MS as described above, after complete disruption of one volume of nanovesicles in 3 volumes of acetone and PL precipitation.

T was quantified by absorbance at 275 nm upon complete disruption of one volume of nanovesicles in 500 volumes of ethanol. The absorption of the sample was compared to a standard curve prepared with T_{RP} diluted in ethanol. The standard curve was linear in the range 0.015 and 0.183 mg/ml, with correlation coefficient of 0.999.

PL were quantified by the colorimetric phosphate assay of Böttcher et al, 1961.

Size (Z-average), polydispersity index (PDI) and zeta potential of nanovesicles were determined by dynamic light scattering (DLS) and phase analysis light scattering (PALS), respectively, using a nanoZsizer device (Malvern Instruments, Malvern, UK). Samples were diluted 1:20 in Tris-HCl buffer for size and Z potential measurements.

Size exclusion chromatography

Size exclusion chromatography was performed on Sephadex G-25, using the minicolumn centrifugation technique. Briefly, 150 µl aliquots of *T*-nanovesicles and *T* emulsion were seed on 3 ml syringe filled with Sephadex G-25 and centrifuged for 3 min at 700 g. Five fractions were obtained after elution with 150 µl of Tris-HCl buffer. The elution profile was determined by quantifying each fraction *T* and PL as described above.

Laurdan generalized polarization (GP) and fluorescence anisotropy (FA)

The order and fluidity of the nanovesicles bilayer were determined by GP and FA of laurdan, respectively, according to (Altube et al, 2017). Briefly, void nanovesicles or *T*-nanovesicles were labelled with laurdan by mixing 10 µl of 120 mM laurdan in methanol with a sufficient volume of nanovesicles to render a 1:20 mol:mol laurdan:PL ratio. Nanovesicles composed of SPC:TPA 1:1 w:w (A) or SPC only (L), prepared as described above, were used as control. The measurements were carried out in LS 55 spectrofluorometer, PerkinElmer.

GP was calculated using the following equation: $GP = (I_{440} - I_{490})/(I_{440} + I_{490})$ where I_{440} and I_{490} are the fluorescence intensities at λ_{em} = 440 nm and λ_{em} = 490 nm, respectively, obtained from the spectra between 400 and 600 nm at λ_{ex} = 364 nm ($Slit_{ex}$: 5.0 nm and $Slit_{em}$: 5.0 nm. Scan speed: 100 nm/min)

FA was calculated using the spectrofluorometer software according to the following equation: $FA = (I_0-GI_{90})/(I_0+2GI_{90})$ where I_0 and I_{90} are the fluorescence intensities at

λ_{em} = 440 nm with λ_{ex} = 364 nm and excitation polarizer oriented at 0 and at 90°, respectively. The correction factor G was obtained from the ratio of the emission intensity at 0 and 90° with the excitation polarizer oriented at 90 ° (after the subtraction of scattered light).

Thermal analysis

Phase transition temperature (Tt) and associated change of enthalpy (ΔH) of A80, L80, A80-*T* and L80-*T* were determined by differential scanning calorimetry (DSC), from −80 to 50 °C at 5 °C/min rate, in a Mettler Toledo DSC 30. A and L nanovesicles were used as control.

Morphology

Morphology of A80 and A80-*T* was conducted by cryo-transmission electron microscopy (cryo-TEM). Samples were prepared in a controlled environment vitrification system Vitrobot Mark IV (Thermo Fischer Scientific, MA, USA) with controlled temperature (22 °C) and humidity (100%). Images were acquired on a TALOS F200C (Thermo Fischer Scientific, MA, USA) instrument, operating at 200 kV using a CMOS camera Ceta 16M 4k x 4k pixels (Thermo Fischer Scientific, MA, USA). Images were not processed after acquisition. Sample preparation and data acquisition were performed at the Electron Microscopy Laboratory (LME)/Brazilian Nanotechnology National Laboratory (LNNano).

Stability upon storage

The colloidal stability of A80-*T*, L80-*T* and *T* emulsion was determined after 90 days storage at 4 ºC. *T* quantification, nanovesicles size, PDI and Z potential before and after storage were determined as stated before.

Macrophage cytotoxicity

Immortalized murine macrophages J774A.1 (ATCC® TIB-67™) were supplied by Dra. Erina Petrera, Facultad de Ciencias Exactas y Naturales, Universidad Nacional de

Buenos Aires, Argentina. J774A.1 were routinely cultured in RPMI supplemented with 10% FBS, 1% antibiotic-antimycotic and 2 mM glutamine at 37 °C in 5% CO_2 and 95% humidity.

Cell viability upon treatment with A80, A80-*T*, L80, L80-*T* and *T* emulsion was measured by MTT assay. Briefly, J774A.1 cells were seeded in 96-well plates at a density of 5×10^4 per well and grown for 24 h. Then, cells were incubated with 100 µl of different concentration of formulations diluted in fresh medium with 5% FCS. The concentrations assayed were 0.1, 0.4 and 2.0 mg/ml of *T* for A80-*T*, L80-*T* and *T* emulsion. The concentrations of empty nanovesicles were 0.2, 0.5 and 2.6 and 0.2, 1.0 and 5.0 mg/ml of PL for A80 and L80, respectively. After 24 h of incubation, cells were washed with phosphate buffer saline (PBS) and 100 µl of 5 mg/ml MTT solution was added to each well. After 3 h of incubation, the MTT solution was removed, the insoluble formazan crystals were dissolved in dimethyl sulfoxide, and absorbance was measured at 570 nm in a microplate reader (Cytation 5 BioTeck, Winooski, VT, USA). The cell viability was expressed as a percentage of the cells grown in medium.

Antibacterial activity

Bacterial strains and growth conditions

The reference *Staphylococcus aureus* American Type Culture Collection (ATCC) 25923 strain and four clinical methicillin-resistant *S. aureus* (MRSA) isolates (Cordobes clone, DOS90, DOS61 and DOS59), obtained and characterized by the Department of Microbiology, Parasitology and Immunology, Faculty of Medicine, University of Buenos Aires as described in Lattar et al, 2012, were used in this study.

Bacteria were stored in TSB with 20% glycerol at −80 °C until use. All cultures were grown in TSB supplemented with 0.25% w/v glucose (TSB glucose) at 37 °C with shaking at 200 rpm overnight before testing.

Growth of planktonic S. aureus, determination of MIC_{90} and MBC

The growth of *S. aureus* after 24 h of incubation with *T* emulsion and *T*-nanovesicles was determined by optical density (OD) at 595 nm. Briefly, two fold dilutions of samples were prepared in TSB glucose, and 80 µl were added to wells in 96-well plate. Subsequently, *S. aureus* culture was diluted to obtain an average concentration of $1x10^6$

colony forming units (CFU)/ml and 20 µl of bacterial inoculum was added to each well. Immediately and 24 h after incubation at 37 °C, OD was measured at 595 nm in Multiskan EX plate reader (Thermo Fisher, MA, USA). Inoculum placed in TSB glucose medium was used as control without treatment and vancomycin was used as standard positive control. The percentage of bacterial growth was calculated respect the growth of control without treatment as follows: % growth = ($OD_{24sample}$ - $OD_{0sample}$)/($OD_{24control}$- $OD_{0control}$) * 100; where $OD_{0sample}$ and $OD_{24sample}$ are OD at 0 h and after 24 h incubation of *S. aureus* with samples, respectively; $OD_{0control}$ and $OD_{24control}$ are OD at 0 h and after 24 h of control, respectively. Each sample was assayed in triplicate and in two independent experiments.

The minimum inhibitory concentration 90 (MIC_{90}) was defined as the lowest concentration of samples that inhibits 90% growth respect to the control in TSB glucose. MIC_{90} was determined by growth results as the minimum concentration in which growth was ≤ 10%.

Minimum bactericidal concentration (MBC) was determined by plating 10 µl from each well with growth ≤ 10% on TSB agar plates. After 24 h incubation, the MBC was regarded as the lowest concentration where no colonies were observed on the agar plates.

Effect on biofilm formation

Inhibition of biofilm formation was determined according to Mishra and Wang (2017). Supernatants of the microplate used for growth experiment were removed and the biomass of biofilm was determined by staining with crystal violet. Briefly, after two washes with sterile PBS, the 96-well plate was dried at 37 °C. The biofilm was fixed with methanol for 15 min. Then, methanol was removed, and the plate was allowed to dry again at 37 °C. Then 1% w/v crystal violet was added and after 20 min, two washes were carried out with distilled water and the plate was allowed to dry for 30 min at 37 °C. Subsequently, stains were solubilized with 30% v/v acetic acid and absorbance of crystal violet at 595 nm (Abs_{CV}) was measured. Abs_{CV} was relativized to the final culture density (OD_{24h} - OD_{0h}) calculated before staining with crystal violet.

Disruption of established biofilm

Firstly, *S. aureus* biofilms were prepared. Briefly, 200 µl of bacterial inoculum, prepared as described above, was incubated at 37 °C in 96-well plates. After 24 h, the supernatants were removed, and biofilm washed with sterile physiological solution. *T*-nanovesicles, *T* emulsion, empty nanovesicles and vancomycin were diluted in TSB glucose to obtain a final concentration of 4 mg/ml *T*, 5 mg/ml PL for A80, 10 mg/ml PL for L80 and 32 µg/ml vancomycin, respectively. Aliquots of 100 µl were added to biofilms and incubated for other 24 h at 37 °C. As a control without treatment, 100 µl of TSB glucose medium was added to *S. aureus* biofilm. After incubation, the supernatants were removed, biofilm was stained with crystal violet and Abs_{CV} was determined as described above.

The % of biofilm disruption was calculated as 100 – ($Abs_{CV}/Abs_{CVcontrol}$ * 100) where Abs_{CV} refers to absorbance of crystal violet after incubation of the biofilm with sample and $Abs_{CVcontrol}$ refers to the average of absorbance of control without treatment. Each sample was assayed in septuplicate and in two independent experiments.

Statistical analysis

Statistical analyses were performed by independent two-way analysis of variance (ANOVA) followed by Dunnet's multiple comparisons test or one-way ANOVA followed by Tukey's multiple comparisons test, using Prisma 4.0 Software (Graph Pad, San Diego, CA, USA). p-value less than 0.05 was considered statistically significant. *p < 0.05; **p < 0.01; ***p < 0.001; ****p < 0.0001.

Results

Characterization of T by GC/MS

The chemical composition of an EO can significantly vary according to several factors: the plant organ from which it is extracted, time of cultivation and harvest, climatic conditions of place of cultivation, and extraction method, among others (Angioni et al, 2006). Here the compositions of *T* and T_{RP} as determined by GC/MS are shown in Table 1. The major components of *T* were thymol (30.2%), *p*-cymene (22.9%), α-terpineol (12.4%) and linalool (10.2%). The reduced pressure barely altered

the percentual composition of T_{RP} compared to *T*, slightly increasing the thymol (35.4%) relative content.

Structural features of T-nanovesicles

Initial attempts to prepare nanovesicles made of lipid and *T* only failed, since the resultant lipid films could not be suspended upon buffer addition, even at different initial (*T*:lipid) ratios [data not shown]. Stable homogeneous suspensions were achieved however, only with ternary mixtures of lipid, *T* and P80. The PL:P80 ratio remained above 1:2.75 mol:mol (1:4 w:w); below which the P80 saturates the bilayer, solubilizing the PL and generating mixed micelles (Simões et al., 2005). It was observed also that regardless of the initial composition, only highly lipid concentrated *T*-nanovesicles [80 and not 40 mg/ml PL] remained colloidally stable in time. Remarkably, the suspension stability depended on the initial (*T*:lipid) ratios and lipid composition. Aqueous suspension of bilayers made of SPC:P80:*T* 1:0.75:0.3 w:w (L80-*T*) was homogeneous (Fig. 1A) but bilayers made with double quantity of *T* (SPC:P80:*T* 1:0.75:0.7 w:w) rapidly formed two phases (Fig. 1B). However, by replacing half of SPC by TPA (SPC:TPA:P80:*T* 0.5:0.5:0.75:0.7 w:w, A80-*T*) the resulting homogeneous suspension remained stable in time (Fig. 1C). The theoretical concentration of L80-*T* and A80-*T* were 27.5 and 55 mg/ml *T*, with theoretical ratios of *T*/PL 27.5/80 [0.34] and 55/80 [0.68], respectively.

The structural features of *T* nanovesicles are detailed in Table 2. Remarkably, L80-*T* and A80-*T* at 55 - 58 mg/ml PL solubilized 22.0 ± 0.6 mg/ml and 41.6 ± 14.6 mg/ml *T* respectively, meaning loses in the order of 20-30% PL mass during nanovesicles extrusion.

Polysorbate 80 molecule is a multi-headed structure, with four extended hydrophilic moieties, one of which has a tagged alkyl chain, that constitutes micelles of around 60 molecules, displaying a radius of gyration of 26.2 Å and a physical radius, determined from both the radius of gyration and atomic density, of about 35 Å (Amani et al, 2011). *T* emulsion (T_{RP} in Tris-HCl buffer with 1% w/v P80) showed a majoritarian population of (96%) 392 ± 33 nm and another (4%) of 4944 ± 320 nm hydrodynamic size, considerably higher than nanovesicles, consistent with nano and micro emulsion droplets.

Potential changes in *T* composition upon loaded in nanovesicles were also surveyed. It was found that thymol was significantly increased at expenses of decreasing more volatile components (54.1% in A80-*T* and 52.5% L80-*T*) [data not shown]. This would signify that the effects of reduced pressure differed according to the chemical environment of *T* paradoxically, within nanovesicles the changes in relative composition were higher than in the oil form.

Fig. 2A showed that upon eluted by Sephadex-G25 size exclusion chromatography, the *T* emulsion microdroplets were collected in the first fraction [void volume]. The A80-*T* and L80-*T* elution profiles of *T* and PL were coincident (Fig. 2B and C), suggesting that *T* remained associated to nanovesicles during elution, indicating colloidal stability in front to dilution.

The GP and FA of laurdan on the other hand, showed that the presence of P80 profoundly modified the structure of L bilayers, that became more disordered and fluid. Opposing, P80 turned the A bilayers more ordered, while their fluidity was unaffected (Fig. 3A and B). The hydrophilic/lipophilic balance of P80 is 15, and acts as an o/w emulsifier, with relatively low tendency to interact with the lipid environment (El Maghraby et al, 2004). *T* could only be retained in nanovesicles bilayers when P80 was added, and *T* had an almost negligible effect on bilayer order and fluidity. Such apparent higher affinity of *T* by P80 suggests that probably *T* partitioned in P80 moieties present in nanovesicles bilayers, instead of in PL.

The effect of P80 and *T* on the thermotropic behaviour of A and L bilayers was determined by DSC. The Tt of the lipid bilayer of A was -24.94 °C, with a ΔH of 84.4 J/g PL (Fig. 4 and Table 3). While the presence of P80 induced a significant decrease of ΔH to 0.8 J/g, the Tt remained almost invariant at - 23.79 °C, the addition of *T* in A80-*T*, induce a small peak at -51.06 °C.

The Tt of the lipid bilayer of L was -25.14 °C with a ΔH of 81.4 J/g of PL. As previously determined in Perez et al, 2016 for SPC:P80 1:0.5 w:w, the phase transition of the SPC:P80 1:0.75 w:w was eliminated.

Cryo-TEM images of A80 and A80-*T* showed spherical vesicles (Fig. 5 A and B), and no aggregates or micelles were observed. Some small nanovesicles were observed within larger vesicles.

Stability upon storage

T emulsion resulted highly unstable; upon 24 h at 4 °C, 2 phases were formed. In contrast, L80-*T* and A80-*T* were colloidally and chemically stable, maintaining size, PDI, Z potential and *T* concentration for at least 90 days (Fig. 6 A and B)

Macrophage cytotoxicity

The J774A.1 macrophages viability was determined upon 24 h of incubation with A80, A80-*T*, L80, L80-*T* and *T* emulsion. It was found that the cell viability was decreased as the PL concentration of A80 increased (Fig. 7). The same trend was observed for A80-*T*, excepting that the presence of *T* in nanovesicle bilayer caused a more pronounced decrease in cell viability close to 90% at 0.4 mg/ml *T*. L80 had no deleterious effect on cell viability in the tested range, but 0.4 mg/ml *T* of L80-*T* decreased cell viability close to 70%. Finally, 0.4 mg/ml *T* emulsion decreased cell viability close to 100%. Taken together, these results show that from 0.4 mg/ml *T* a significantly decreased of macrophages viability was produced with independence of the formulation.

Antibacterial activity (MIC_{90} and MBC) on planktonic S. aureus

As expected, the standard antibiotic vancomycin decreased the growth of all *S. aureus* strains. Empty nanovesicles on the other hand, had no effect on the growth of *S. aureus* (Fig. 8 A), but *T*- nanovesicles and *T* emulsion decreased the growth of all *S. aureus* strains (Fig. 8 B-F). (Fig. 1S).

Specifically, MIC_{90} of vancomycin was between 4-8 µg/ml and resulted comparable to MIC_{90} of L80-*T* and *T* emulsion, that was > 4 mg/ml. Notably, the MIC_{90} of A80-*T* was 2 mg/ml on all *S. aureus* strains (Table 4).

On the other hand, MBC was > 4 mg/ml *T* for *T*-nanovesicles and *T* emulsion. However, a slight decrease in the number of CFU/ml was observed in all strains after incubation with 4 mg/ml A80-*T*. These results suggest that A80-*T* would be the most effective antiplanktonic agent. MBC of vancomycin was 16 µg/ml against ATCC 25923 and DOS61 strains, 32 µg/ml for Cordobes clone, and > 32 µg/ml for DOS90 and DOS59 strains.

Effect on biofilm formation

We found that L80-*T* did not inhibit the biofilm formation, but *T* emulsion at 2 mg/ml significantly inhibited biofilm formation of Cordobes clone and DOS90 strains and at 4 mg/ml inhibited ATCC 25923, DOS61 and DOS59 (Fig. 9). Remarkably however, A80-*T* at only 0.5 mg/ml significantly inhibited ATCC25923, DOS90 and DOS61 strains biofilm formation, whereas 1 mg/ml and 2 mg/ml were required to inhibit the Cordobes clone and DOS59 biofilms, respectively. Overall, the anti-biofilm formation activity was maximal for A80-*T*, at values lower than or equal to MIC_{90} and lower than MBC. This could be ascribed to its lower size and higher structural stability compared to the *T* emulsion and or to the *T*/PL ratio of A80-*T* two folds higher than that of L80-*T*. Impairing the biofilm formation may facilitate the further destruction of planktonic bacteria that would be unprotected.

Remarkably, Vancomycin did not significantly inhibit the biofilm formation at any concentration assayed (Fig. 2S).

Disruption of preformed biofilm

Biofilms of different strains of *S. aureus* were prepared and incubated with empty nanovesicles, *T*-nanovesicles, *T* emulsion and vancomycin (Fig. 10).

Empty nanovesicles and L80-*T* did not modify the biofilms biomass compared to untreated control. *T* emulsion and A80-*T* significantly decreased the biomass of the biofilms of *S. aureus* ATCC 25923 strain and of 3 of the 4 clinical MRSA isolates. The only strain refractory to biofilm disruption was the Cordobes clone. The disruption of preformed biofilm was thus strain dependent, probably arising from structural features hampering or facilitating the access of particulate material to bacterial targets.

Vancomycin, despite of tested at concentration 4 and 8 folds higher than MIC_{90}, did not reduce the biofilm biomass of any *S. aureus* strains.

Discussion

EOs are widely used as natural preserving agents to control lipid oxidation and microorganisms induced deterioration in food. In the last 5 years, the rise of nanotechnology on the food, livestock feed and pharmaceutics fields aroused a growing interest on loading techniques and performance of EO or isolated components in nanoparticulate material (Rai et al., 2017; Morilla and Romero, 2018).

In this work, a colloidally stable formulation of *T* in nanovesicles was developed and its antiplanktonic bacterial and antibiofilm activities were determined. To the best of our knowledge, this is the first report of the loading of the essential oil *T* (and not the isolated thymol) in nanoparticles aimed for therapeutic use. Gortzi et al., 2006 for instance, loaded distinct species of *Thymus* gender EOs in multilamellar vesicles made of phosphatidylcholine:cholesterol:phosphatidylglycerol:*Thymus spp* EO 5:1:0.5:0.8 w:w prepared by the hydration of the thin lipid film. The formulations however, lacked structural characterization and the final EO concentration was not determined. More recently, *T* or *T*/K proteinase were loaded in lipid vesicles of SPC:cholesterol:*T* 1:0.2:0.25 w:w to be used in food industry aiming to decrease the *E. coli* O157:H7 biofilms on the surface of vegetables (Cui et al., 2016). Here the nanovesicles were prepared by the hydration of thin film method, a technique involving solvent evaporation at reduced pressure. Though because of its simplicity the method is popularly used, the reduced pressure may affect the EO composition. Because of that, firstly the *T* composition was checked by GC/MS before and after submitted to reduce pressure or loading it in vesicles. It was found that the reduced pressure did not significantly modify the percentage of majoritarian components *p*-cymene, α-terpineol and linalool did not change while thymol was slightly concentrated. Regarding to the interaction between PL and EO components, studies by nuclear proton magnetic resonance spectroscopy (H-NMR) indicate that thymol and other phenols accommodate between the choline and glycerol backbone, close to the polar head of phosphatidylcholine and the first atoms of the acyl chains. The more lipophilic compounds prefer a deeper bilayer insertion to finally diminish the mobility of the hydrocarbon chains (Reiner et al., 2013a). Fluorescence anisotropy studies have also shown that phenols decrease the bilayers microviscosity (Reiner et al., 2013b). Discrepancies on the effect of EO on order and fluidity of PL bilayers are explained by the fact that our findings regard to the interaction of a complex molecular mixture conforming the *T*, instead of isolated molecules. In our experience, the thin film method did not allow partitioning EO into lipid films to render colloidally stable formulations. To overcome such issue and avoid the generation of two phases, a surfactant was included to the lipid bilayers. The non-ionic P80 surfactant is a widely used solubilizing agent and stabilizing/emulsifier in pharmaceutic formulations. P80 inserts in the lipid bilayer with its oleate (lipophilic) residua aligned in parallel with the acyl chains while its big polar head (containing nearly 20 units polyoxiethylene) oriented to the PL head

(El Maghraby et al., 2004). The increased volume of the headgroup would facilitate the fitting of the thymol in that area. Our mixed bilayer made of PL and P80 enabled to achieve aqueous dispersions of 22 mg/ml *T* and by replacing half SPC by archaeolipids, it was raised to 41 mg/ml *T*, nearly 2.5 folds higher than *T* emulsion (that dropped from 55 to 16 mg/ml *T* upon 24 h) or 24 folds higher than the 1.7 mg/ml *T* of formulations developed by Cui. Remarkably, the presence of archaeolipids not only provided higher *T*/PL ratios but of a longer structural stability during storage.

Skin bacterial infections are highly common and involve mostly Gram-positive bacteria; those caused by MRSA comprise nearly 50% of the isolates from *S. aureus* (Cardona and Wilson, 2015). The reason why leg venous, pressure, and diabetic foot ulcers become chronic is the formation of biofilms, responsible for permanent inflammation in the wound and lengthy healing (Percival et al., 2012). Pathogenicity of antibiotic resistant *S. aureus* infections acquired in hospitals and community rely in part on the biofilm formation. Biofilms are structured consortium of bacteria embedded in a self-produced polymer matrix consisting of polysaccharide, protein and DNA (Percival et al., 2012). *S. aureus* biofilms are present in multiple infections associated to medical dispositive, osteomyelitis, chronic skin wounds, periodontitis, chronic sinusitis, endocarditis and eye infections (Archer et al, 2011). Treatments against early established biofilms render the best results (Høiby et al, 2015). However, the biofilms capacity to persist long periods without being detected or eradicated by the host immune system makes the diagnosis difficult. The only current effective methods are physical removal of the infection source; the antibiotic therapy is poorly effective to defeat the infection (Høiby et al, 2015). Finally, the phenotype of bacteria in biofilms is different from that of planktonic; but even the sensitive to methicillin strains may tolerate much higher concentrations of antibiotics than isogenic planktonic ones, which makes difficult to eradicate infections. Taken together, these reasons make the search for new anti-biofilm forming MRSA agents, of outmost importance.

Although more research and clinical trials are needed, it has recently been proposed to replace conventional antibiotics with EOs (Swamy et al, 2016). There is also growing interest in the synergistic combination of conventional antibiotics with EOs to combat antibiotic resistance (Lahmar et al, 2017).

The MIC and MBC of *T* against planktonic *S. aureus* recalled by other authors is highly variable, probably owed to the different sources and obtaining methods of *T* and to the presence or not of stabilizing agents, as well to the different strains of *S. aureus*

(see Table 5). Such variability difficult accurate comparisons. Kavanaugh and Ribbeck, 2012 for instance, determined a higher efficacy of *T* compared to oxacillin and methicillin antibiotics, at a minimum concentration for biofilm eradication of 1.7% v/v *T* (7 mg/ml *T*), by measuring CFU/ml in biofilms from a clinical MRSA strain. Al-Shuneigat et al., 2014 on the other hand, determined that the minimum concentration that caused a 30% decrease in Abs_{CV} of MRSA and methicillin sensitive *S. aureus* clinical strain biofilm was 0.25% v/v *T* (1.1 mg/ml *T*). There are few reports combining accurate analytical structural description of the carrier nanoparticles for *T*, together with its antimicrobial activity. One of them is Gortzi et al, 2006 that loaded *Thymus* spp *(T. longicaulis* and *T. ocheus)* EO in nanovesicles, to observe by disk diffusion, higher activity of EO in nanovesicles than free EO against planktonic *S. aureus*.

Our results suggest that A80-*T* may be used to magnify the antimicrobial activity of *T* against planktonic and in MRSA biofilm. We found that while L80-*T* at 4 mg/ml *T* was inactive, *T* emulsion and A80-*T* significantly decreased the biofilm biomass of a *S. aureus* reference strain and 3 MRSA strains. Nonetheless, despite of its A80-*T* comparable disrupting biofilm activity, the colloidal stability of *T* emulsion was poor, collapsing 24 h after prepared. Finally, the idea of employing A80-*T* as antimicrobial agent deserves to be carefully considered in the light of the pronounced cytotoxicity of *T* emulsion and *T*-nanovesicles on J774A.1 macrophages, at concentrations lower than the MIC. Oliveira et al, 2017 had already reported a reduction of 20 to 40% the viability of RAW 264.7 macrophages upon 5 min incubation with a *Thymus vulgaris* glycolic extract at concentrations below those causing a significant diminution of CFU/ml in *S. aureus* ATCC 6538 biofilms. Macrophages act as first line of defence against microbes and are critical to amplify and orchestrate the activation/recruitment of immune cells. *S. aureus* is capable of surviving and persisting within different types of host cells, including macrophages and keratinocytes (Jakab and Green, 1976; Kintarak et al, 2004). In such cases, the pronounced toxicity of A80-*T* on macrophages may help to eradicate the infection.

Conclusions

Overall, because of its lower MIC_{90} against planktonic bacteria, higher antibiofilm formation capacity and stability during storage, A80-*T* resulted better antibacterial agent than *T* emulsion and L80-*T*. These results open new avenues to explode the A80-*T* (or

other structurally related macrophage targeted *T* loaded nanoparticles) antimicrobial intracellular activity.

Acknowledgments

The authors would like to thank to LME/LNNano for the use of electron microscopy facility and technical support. This work was supported by Secretaria de Investigaciones Universidad Nacional de Quilmes under Grant Nanomedicinas-2. NP, MS and JA have fellowships from National Council for Scientific and Technological Research (CONICET). ELR, MJM, APP and FB are members of the Research Career Program from CONICET.

Conflict of interest

The authors declare that there are no conflicts of interest.

References

Al-Shuneigat, J., Al-Sarayreh, S., Al-Saraireh, Y., Al-Qudah, M., Al-Tarawneh, I. 2014. Effects of wild *Thymus vulgaris* essential oil on clinical isolates biofilm-forming bacteria. J. Dental Med. Sci. 13, 62-66.

Altube, M.J., Selzer, S.M., de Farias, M.A., Portugal, R.V., Morilla, M.J., Romero, E.L. 2016. Surviving Nebulization-Induced Stress: Dexamethasone in pH-sensitive Archaeosomes. Nanomedicine 11, 2103-2117.

Altube, M.J., Cutro, A., Bakas, L., Morilla, M.J., Disalvo, E.A., Romero E.L. 2017. Nebulizing novel multifunctional nanovesicles: the impact of macrophage-targeted-pH-sensitive archaeosomes on a pulmonary surfactant. J. Mater. Chem. B 5, 8083-8095.

Amani, A., York, P., de Waard, H., Anwar, J. 2011. Molecular dynamics simulation of a polysorbate 80 micelle in water. Soft Matter 7, 2900-2908.

Angioni, A., Barra, A., Coroneo, V., Dessi, S., Cabras, P. 2006. Chemical composition, seasonal variability, and antifungal activity of *Lavandula stoechas L. ssp. stoechas* essential oils from stem/leaves and flowers. J. Agric. Food Chem. 54, 4364-4370.

Archer, N.K., Mazaitis, M.J., Costerton, J.W., Leid, J.G., Powers, M.E., Shirtliff, M.E. 2011. *Staphylococcus aureus* biofilms. Properties, regulation, and roles in human disease. Virulence 2, 445-459.

Bassolé, I.H.N., Juliani, H.R. 2012. Essential oils in combination and their antimicrobial properties. Molecules 17, 3989-4006.

Böttcher, C.J.F., Van Hent, C.M, Pries, C. 1961. A rapid and sensitive sub-micro phosphorus determination. Anal. Chim. Acta 24, 203-204.

Caimi, A.T., Parra, F., de Farias, M.A., Portugal, R.V., Perez, A.P., Romero, E.L., Morilla, M.J. 2017. Topical vaccination with super-stable ready to use nanovesicles. Colloids Surf. B: Biointerfaces, 152, 114-123.

Caimi, A.T., Altube M.J., de Farias, M.A., Portugal, R.V., Perez, A.P., Romero, E.L., Morilla, M.J. 2019. Novel imiquimod nanovesicles for topical vaccination. Colloids Surf. B: Biointerfaces, 174, 536-543.

Cardona, A.F., Wilson, S.E. 2015. Skin and soft-tissue infections: a critical review and the role of telavancin in their treatment. Clin. Infect. Dis. 61, 69-78.

Cui, H., Ma, C., Lin, L. 2016. Co-loaded proteinase K/thyme oil liposomes for inactivation of *Escherichia coli* O157:H7 biofilms on cucumber. Food Funct. 9, 4030-4040.

El Maghraby, G.M., Williams, A.C., Barry, B.W. 2004. Interactions of surfactants (edge activators) and skin penetration enhancers with liposomes. Int. J. Pharm. 19,143-161.

Gonzalez, R.O., Higa, L.H., Cutrullis, R.A., Bilen, M., Morelli, I., Roncaglia, D.I., Corral, R.S., Morilla, M.J., Petray, P.B., Romero, E.L. 2009. Archaeosomes made of *Halorubrum tebenquichense* total polar lipids: A new source of adjuvancy. BMC Biotechnol. 9, 71-83.

Gortzi, O., Lalas, S., Chinou, I., Tsaknis, J. 2006. Reevaluation of antimicrobial and antioxidant activity of *Thymus* spp. extracts before and after encapsulation in liposomes. J. Food Protect. 69, 2998-3005.

Higa, L.H., Schilrreff, P., Perez, A.P., Iriarte, M.A., Roncaglia, D.I., Morilla, M.J., Romero, E.L. 2012. Ultradeformable archaeosomes as new topical adjuvants. Nanomedicine 8, 1319-1328.

Høiby N., Bjarnsholt T., Moser C., Bassi G.L., Coenye T., Donelli G., Hall-Stoodley, L., Holá, V., Imbert, C., Kirketerp, K., Møller, Lebeaux, D., Oliver, A., Ullmann, A.J., Williams, C. 2015. ESCMID guideline for the diagnosis and treatment of biofilm infections 2014. Clin. Microbiol. Infect. 21, 1-26.

Jakab, G.J., Green, G.M. 1976. Defect in intracellular killing of *Staphylococcus aureus* within alveolar macrophages in Sendai virus-infected murine lungs. J. Clin. Invest. 57, 1533-1539.

Kavanaugh N. L., Ribbeck K. 2012. Selected antimicrobial essential oils eradicate *Pseudomonas* spp. and *Staphylococcus aureus* biofilms. Appl. Environ. Microbiol. 78, 4057-4061.

Kintarak, S., Whawell, S.A., Speight, P.M., Packer, S., Nair, S.P. 2004. Internalization of *Staphylococcus aureus* by human keratinocytes. Infect. Immun. 72, 5668-5675.

Lahmar, A., Bedoui, A., Mokdad-Bzeouich, I., Dhaouifi, Z., Kalboussi, Z., Cheraif, I., Ghedira, K., Chekir-Ghedira, L. 2017. Reversal of resistance in bacteria underlies synergistic effect of essential oils with conventional antibiotics. Microb. Pathog. 106, 50-59.

Lattar, S.M., Tuchscherr, L.P., Centron, D., Becker, K., Predari, S.C., Buzzola, F.R., Robinson, D.A., Sordelli D.O. 2012. Molecular fingerprinting of *Staphylococcus aureus* isolated from patients with osteomyelitis in Argentina and clonal distribution of the cap5(8) genes and of other selected virulence genes. Eur. J. Clin. Microbiol. Infect. Dis. 31, 2559-2566.

Mishra, B., Wang, G. 2017. Individual and combined effects of engineered peptides and antibiotics on *Pseudomonas aeruginosa* biofilms. Pharmaceuticals 10.

Morilla, M.J., Romero, E.L. 2018. Essential oil-based nanomedicines against trypanosomatides, In: Rai, M., Zacchino, S., Derita, M. (Eds), Essential Oil and Nanotechnology for Treatment of Microbial Diseases, CRC Press, New York, pp. 296-309.

Oliveira, J.R., Viegas, D.J., Martins, A.P.R., Carvalho, C.A.T., Soares, C.P., Camargo, S.E.A., Jorge, A.O.C., de Oliveira, L.D. 2017. *Thymus vulgaris* L. extract has antimicrobial and anti-inflammatory effects in the absence of cytotoxicity and genotoxicity. Arch. Oral Biol. 82, 271-279.

Percival, S.L., Hill, K.E., Williams, D.W., Hooper, S.J., Thomas, D.W., Costerton J.W. 2012. A review of the scientific evidence for biofilms in wounds. Wound Repair Regen. 20, 647-657.

Perez, A.P., Altube, M.J., Schilrreff, P., Apezteguia, G., Celes, F.S., Zacchino, S., Indiani de Oliveira, C., Romero, E.L., Morilla, M.J. 2016. Topical amphotericin B in ultradeformable liposomes: formulation, skin penetration study, antifungal and antileishmanial activity in vitro. Colloids Surf. B Biointerfaces 139, 190-198.

Rai, M., Paralikara, P., Jogeea, P., Agarkara, G., Inglea, A.P., Deritab, M., Zacchino, S. 2017. Synergistic antimicrobial potential of essential oils in combination with nanoparticles: Emerging trends and future perspectives. Int. J. Pharm. 519, 67-78.

Reiner, G., Fraceto, L.F., de Paula, E., Perillo, M.A., Garcia, D.A. 2013a. Effects of gabaergic phenols on phospholipid bilayers as evaluated by 1H-NMR. J. Biomater. Nanobiotechnol. 4, 28-34.

Reiner, G.N., Delgado-Marín, L., Olguín, N., Sánchez-Redondo, S., Sánchez-Borzone, M., Rodríguez-Farré, E., Suñol, C., García, D.A. 2013b. Gabaergic pharmacological activity of propofol related compounds as possible enhancers of general anesthetics and interaction with membranes. Cell Biochem. Biophys. 67, 515-525.

Simões, S.I., Tapadas, J.M., Marques, C.M., Cruz, M.E.M., Martins, M.B.F., Cevc, G. 2005. Permeabilisation and solubilisation of soybean phosphatidylcholine bilayer vesicles, as membrane models, by polysorbate, Tween 80. Eur. J. Pharm. Sci. 26, 307-317.

Swamy, M.K., Akhtar, M.S., Sinniah, U.R. 2016. Antimicrobial properties of plant essential oils against human pathogens and their mode of action: an updated review. Evid. Based Complement. Altern. Med. 2016.

Tohidpour, A., Sattari, M., Omidbaigi, R., Yadegar, A., Nazemi, J. 2010. Antibacterial effect of essential oils from two medicinal plants against methicillin-resistant *Staphylococcus aureus* (MRSA). Phytomedicine 17, 142-145.

WHO 2017. Global priority list of antibiotic-resistant bacteria to guide research, discovery, and development of new antibiotics. Available online (last access October 2018): https://www.who.int/medicines/publications/global-priority-list-antibiotic-resistant-bacteria/en/

Figure legends

Fig. 1. Aqueous suspension of bilayers made of (A) SPC:T80:*T* 1:0.75:0.3 w:w, (B) SPC:T80:*T* 1:0.75:0.7 w:w and (C) SPC:TPA:T80:*T* 0.5:0.5:0.75:0.7 w:w.

Fig. 2. Size exclusion chromatography elution profile of (A) *T* emulsion, (B) L80-*T* and (C) A80-*T*. Values are expressed as mean ± SD (n = 3).

Fig. 3. (A) Laurdan generalized polarization (GP) and (B) fluorescence anisotropy (FA) in nanovesicles. Values are expressed as mean ± SD (n = 3).

Fig. 4. Thermal analysis by DSC of A, A80, A80-*T*, L, L80 and L80-*T*.

Fig. 5. Cryo-TEM images of (A) A80 and (B) A80-*T*.

Fig. 6. Colloidal and chemical stability of A80-*T* and L80-*T* upon storage, (A) Z-average and PDI (Columns show size and dots show PDI) and (B) % of *T* and Z

potential (Columns show % of *T* and dots show Z potential). Values are expressed as mean ± SD (n = 3).

Fig. 7. Viability of J774A.1 cells upon 24 h incubation with A80, A80-*T*, L80, L80-*T* and *T* emulsion evaluated by MTT assay. Values are express as mean ± SD (n=3).

Fig. 8. Bacterial growth of *S. aureus* strains (A) ATCC 25923, (B) Cordobes clone, (C) DOS90, (D) DOS61 and (E) DOS59, in the presence of different concentrations of *T* emulsion, A80-*T* and L80-*T*. (F) Bacterial growth of *S. aureus* strains incubated with A80 (5 mg/ml PL) and L80 (10 mg/ml PL). Values are expressed as mean ± SD (n = 2).

Fig. 9. Inhibition of biofilm formation by *T* emulsion, A80-*T* and L80-*T* on *S. aureus* stains (A) ATCC 25923, (B) Cordobes clone, (C) DOS90, (D) DOS61 and (E) DOS59. Values are expressed as mean ± SD (n = 2).

Fig. 10. % of biofilm disruption of *S. aureus* strains (A) ATCC 25923, (B) Cordobes clone, (C) DOS90, (D) DOS61 and (E) DOS59, after incubation with 5 mg/ml of PL as A80, 10 mg/ml of PL as L80, 4 mg/ml of *T* as *T* emulsion, A80-*T* and L80-*T* and 32 µg/ml of vancomycin. Values are expressed as mean ± SD (n = 2).

Fig. 1S. Bacterial growth of *S. aureus* strains (A) ATCC 25923, (B) Cordobes clone, (C) DOS90, (D) DOS61 and (E) DOS59 incubated with different concentrations of vancomycin. Values are expressed as mean ± SD (n = 2).

Fig. 2S. Inhibition of biofilm formation by vancomycin on *S. aureus* stains (A) ATCC 25923, (B) Cordobes clone, (C) DOS90, (D) DOS61 and (E) DOS59. Values are expressed as mean ± SD (n = 2).

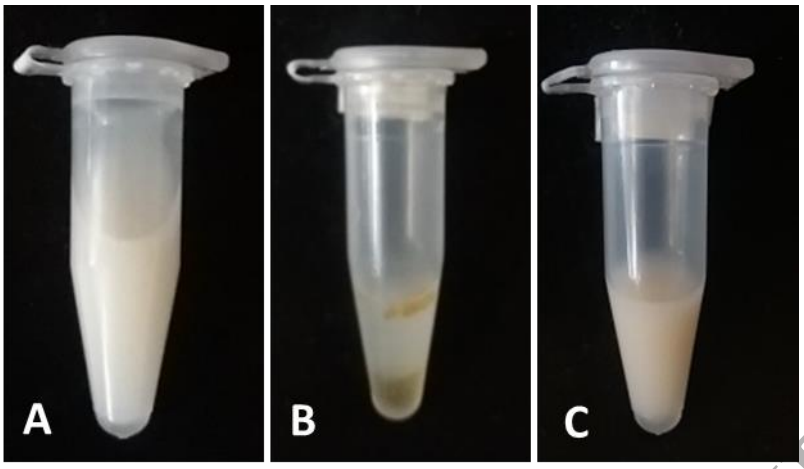

Figure 1

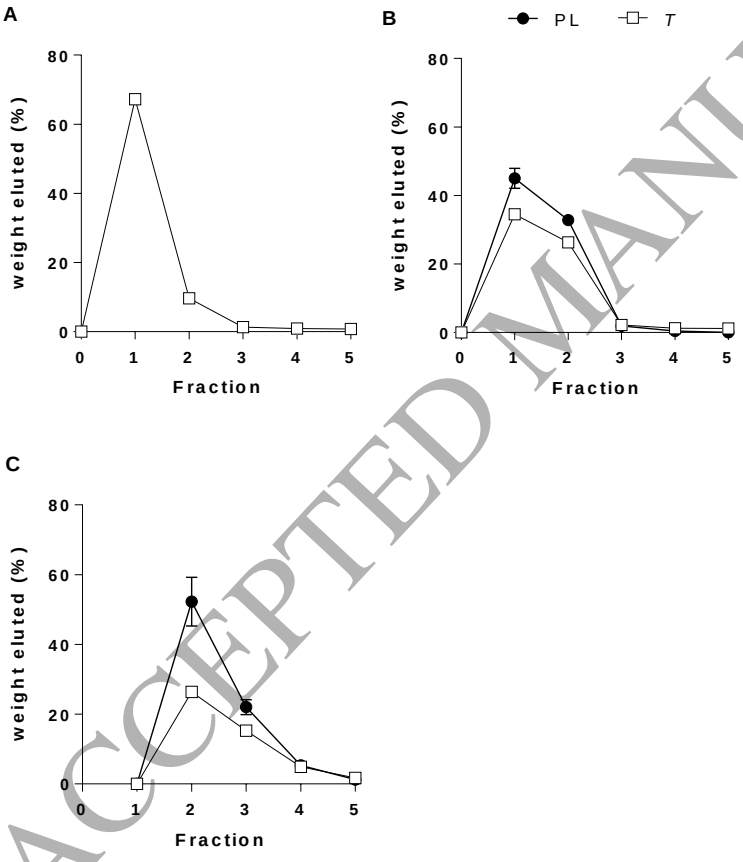

Figure 2

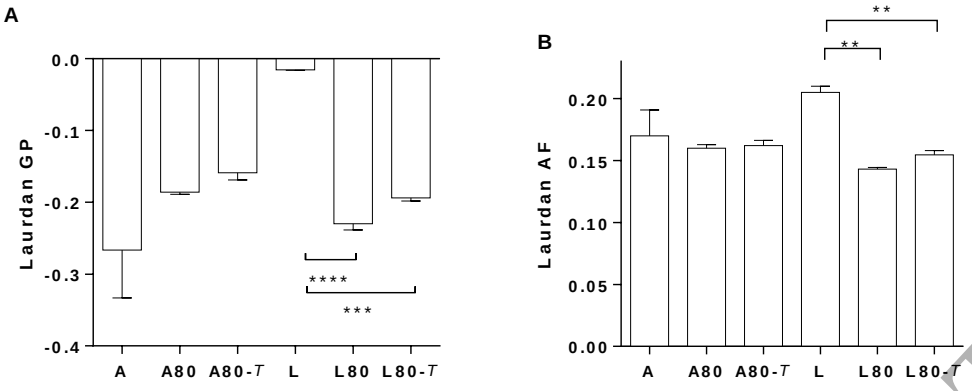

Figure 3

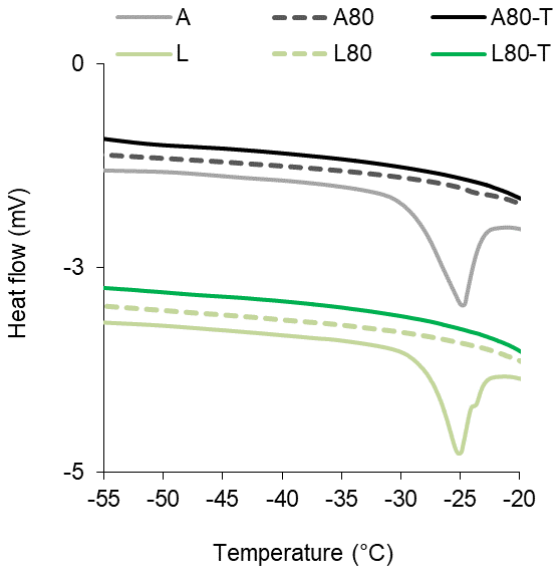

Figure 4

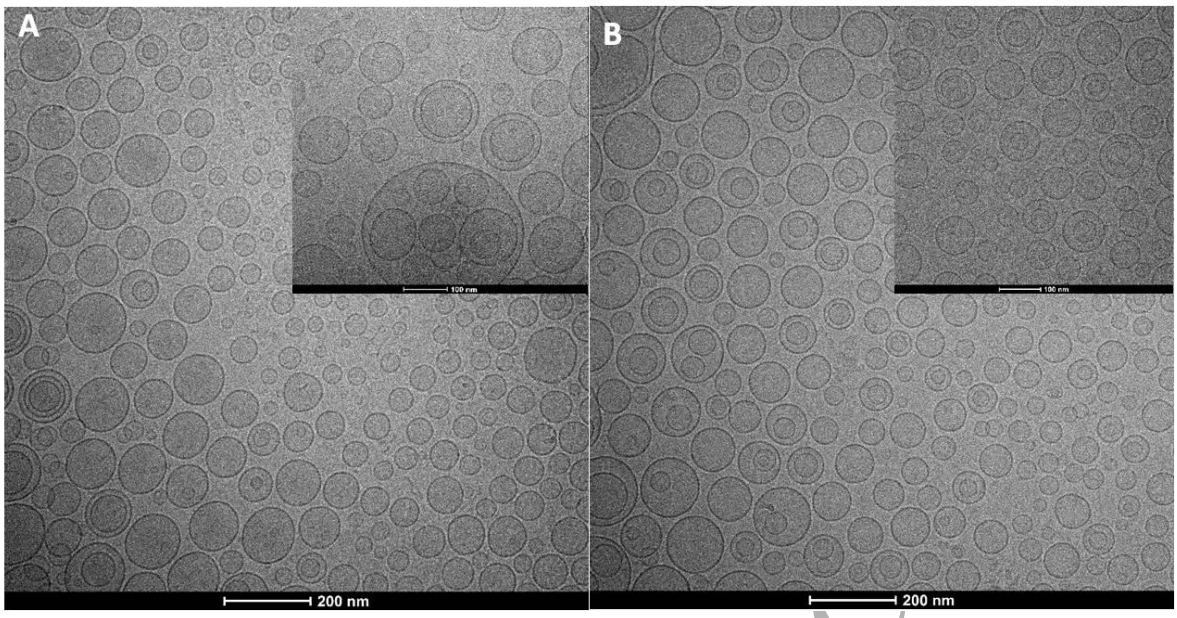

Figure 5

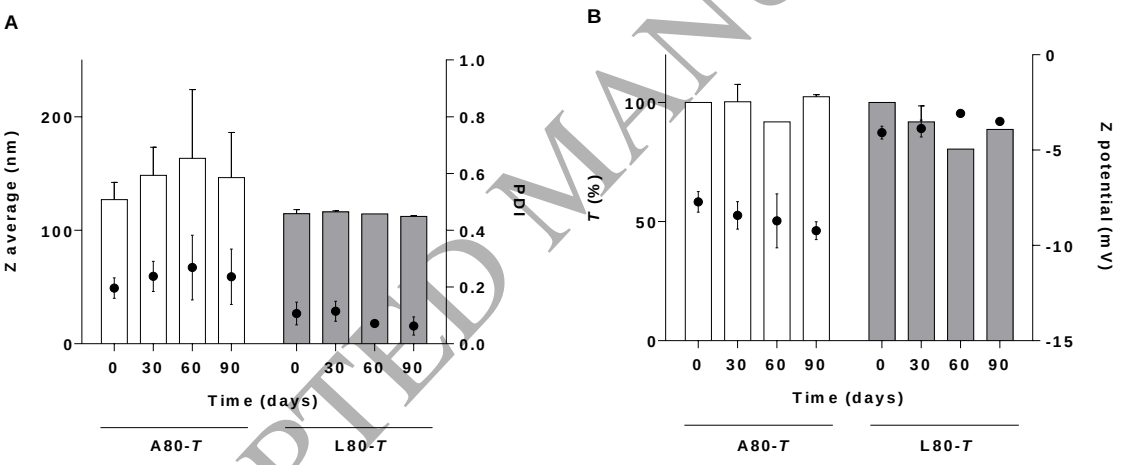

Figure 6

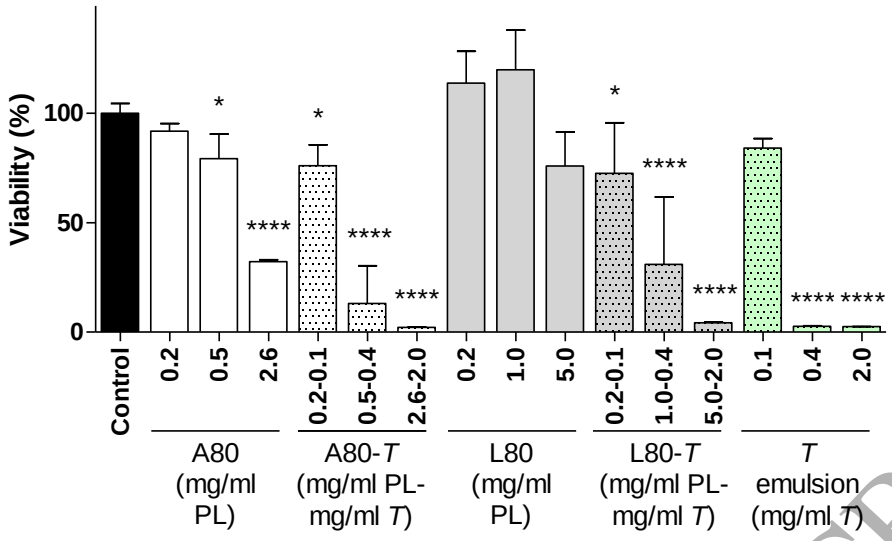

Figure 7

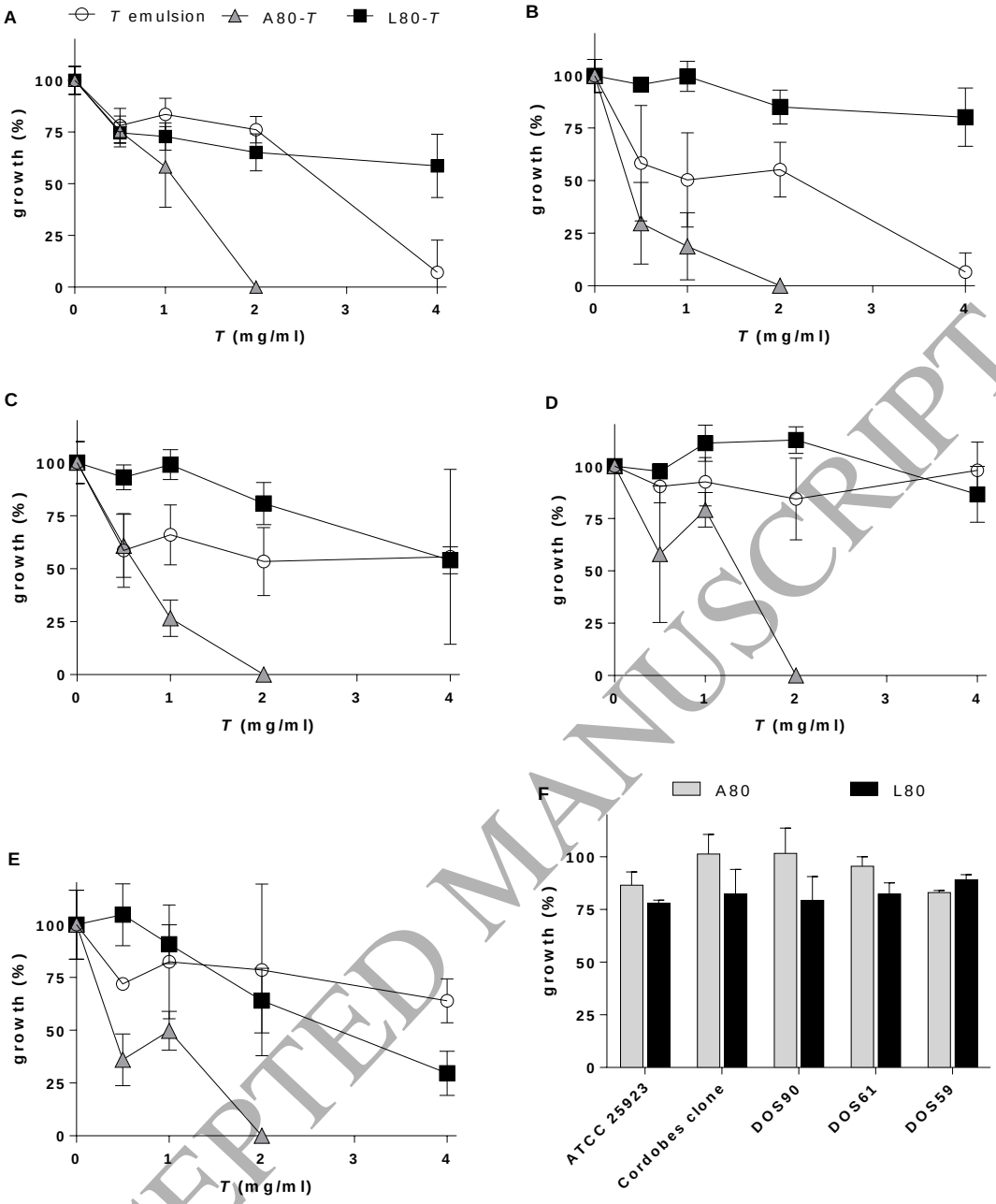

Figure 8

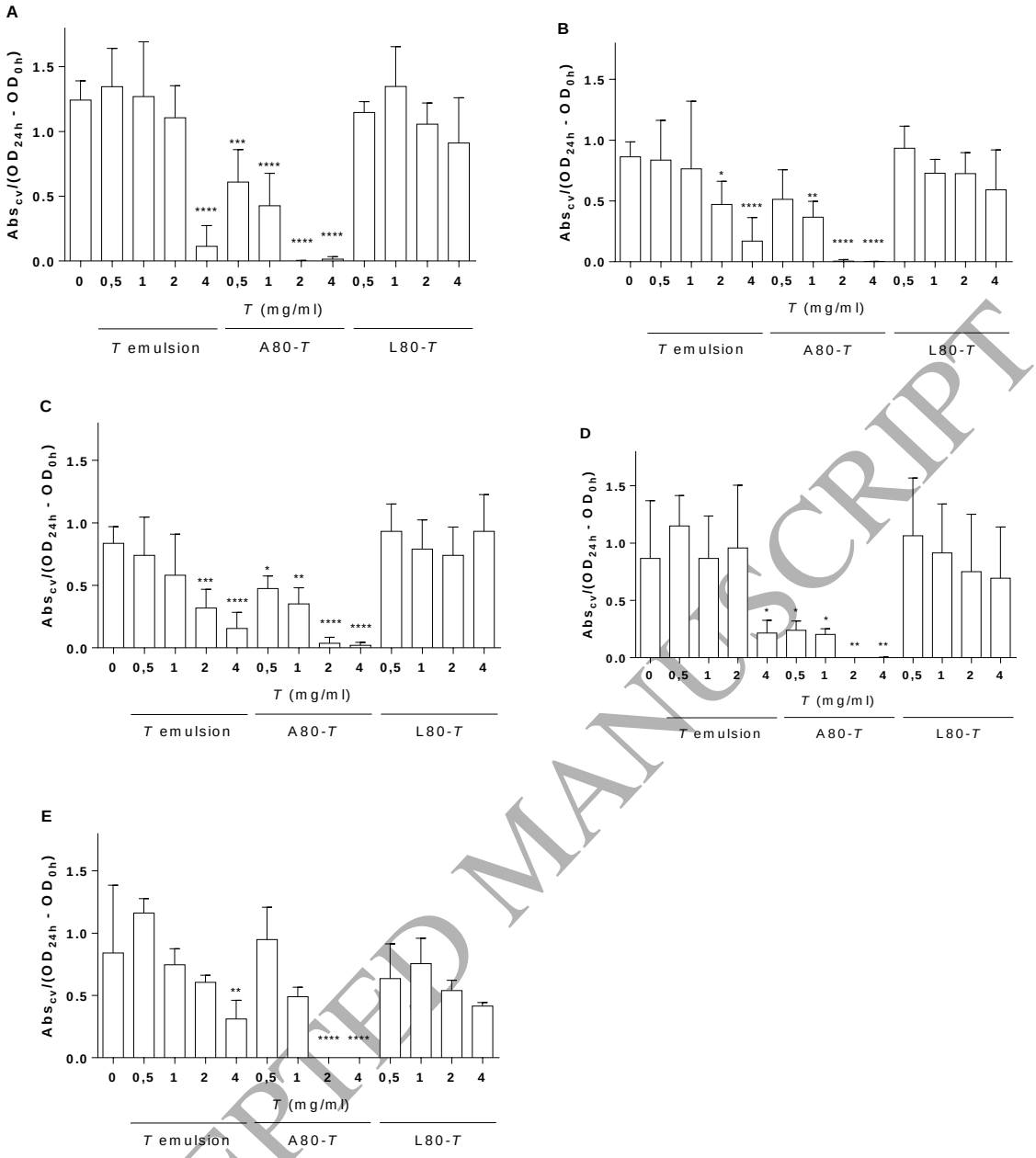

Figure 9

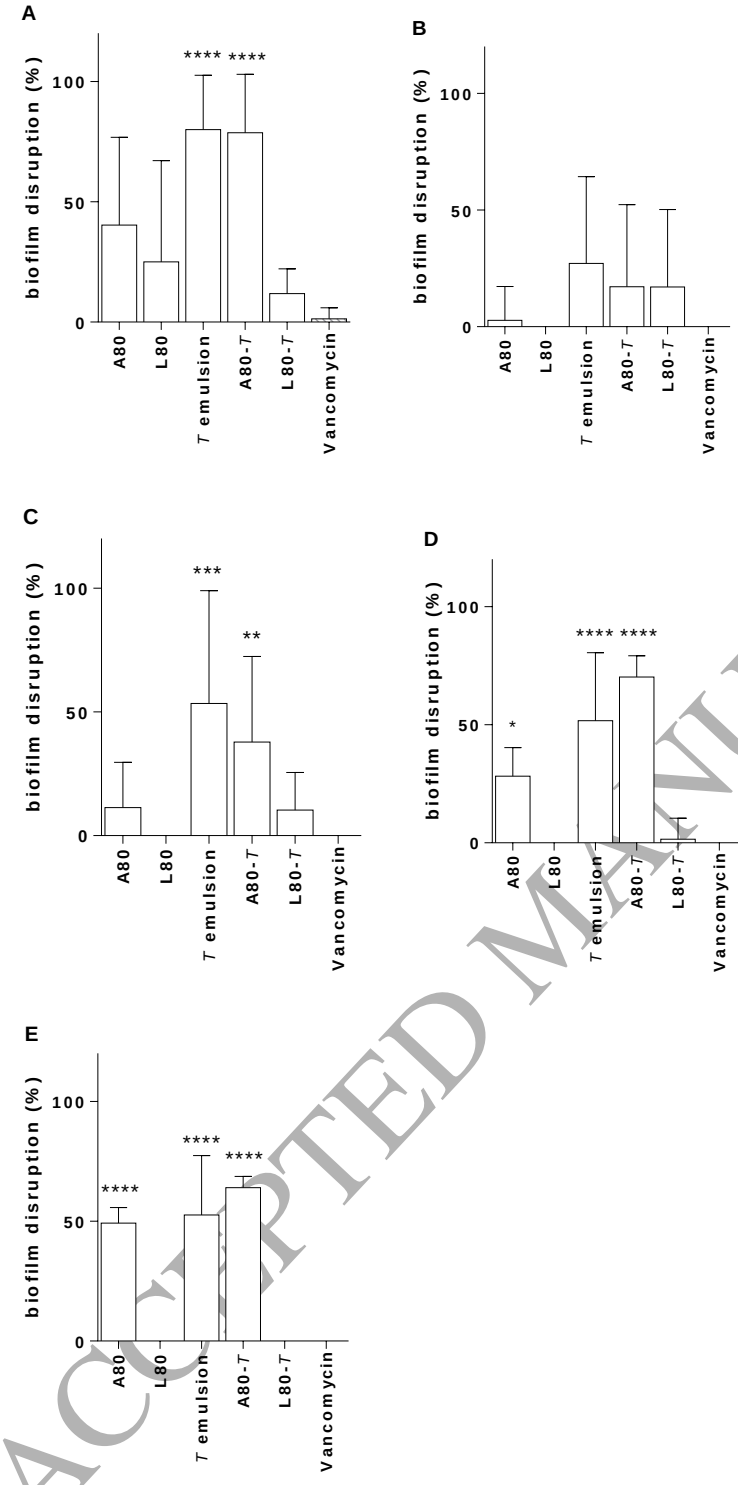

Figure 10

Table 1. Chemical composition of *T* and T_{RP}.

Retention time (min)	Component	*T* %	T_{RP} %
7.815	α-Pinene	3.68	1.82
8.294	Camphene	1.30	0.67
9.244	β-Pinene	0.46	0.19
9.783	Myrcene	1.75	0.98
10.901	*p*-Cymene	22.91	21.02
11.046	Limonene	0.11	0.07
11.125	1.8-Cineol	2.38	1.81
13.559	Linalool	10.21	10.46
14.742	1-Terpineol	1.32	1.29
15.080	β-Terpineol	3.22	3.21
16.667	α-Terpineol	12.42	13.29
16.903	γ-Terpineol	5.01	5.19
20.051	Thymol	30.20	35.40
24.000	β-Caryophyillene	2.05	2.13
	Total	97.02	97.53

Table 2. Composition and structural characteristics of nanovesicles. Values given are mean values of 5 different batches ± standard deviation (SD).

Formulation	Composition	*T* (mg/ml)	Z-average (nm)	PDI	Zeta potential (mV)
L80	SPC:T80 1:0.75 w:w	-	116.9 ± 3.3	0.07 ± 0.02	-2.8 ± 0.9
L80-*T*	SPC:T80:*T* 1:0.75:0.3 w:w	22.0 ± 0.6	114.6 ± 6.4	0.11 ± 0.07	-4.1 ± 0.6
A80	SPC:TPA:T80 0.5:0.5:0.75 w:w	-	121.5 ± 20.2	0.11 ± 0.02	-12.1 ± 1.2
A80-*T*	SPC:TPA:T80:*T* 0.5:0.5:0.75:0.7 w:w	41.6 ± 14.6	129.2 ± 23.0	0.21 ± 0.06	-6.6 ± 1.5

Table 3. Thermotropic parameters of A, A80, A80-*T*, L, L80 and L80-*T*.

Formulation	Tt (°C)	ΔH (J/g PL)
A	-24.94	84.4
A80	-23.79	0.8
A80-*T*	-51.06	6
L	-25.14	81.4

L80	-	-
L80-*T*	-	-

Table 4. MIC_{90} of A80, L80, *T* emulsion, A80-*T*, L80-*T* and vancomycin against *S. aureus*. n=2

Strain of *S. aureus*	MIC_{90} (mg/ml PL)		MIC_{90} (mg/ml *T*)			MIC_{90} vancomycin (µg/ml)
	A80	L80	*T* emulsion	A80-*T*	L80-*T*	
ATCC 25923	>5	>10	>4	2	>4	8
Cordobes clone	>5	>10	>4	2	>4	8
DOS90	>5	>10	>4	2	>4	4
DOS61	>5	>10	>4	2	>4	8
DOS59	>5	>10	>4	2	>4	8

Table 5. Examples of antibacterial activity of *T* (density of *T* was considered 0,915 g/ml to calculated mg/ml from % v/v)

Author	Antibacterial agent	*S. aureus* strain	MIC
Tohidpour et al, 2010	*T* diluted in Muller Hinton with 0.5% v/v of Tween 20	ATCC 25922	0.018 mg/ml
		MRSA clinical strain	0.018-0.037 mg/ml
Al-Shuneigat et al, 2014	*T* diluted in TSB	MRSA clinical strain	2.3 mg/ml
		Methicillin sensitive SA clinical strain	1.1 mg/ml
Kavanaugh & Ribbeck, 2012	*T* diluted in Mueller Hinton broth with 0.1% v/v of T80	MRSA clinical strain	7 mg/ml

Graphical abstract